Iranian Hydraulic Association
Journal of Hydraulics
Vol. 19, No. 4, PP. 11-29, Winter 2025

Research Article
https://doi.org/10.30482/jhyd.2024.423155.1683

Study of Transverse Flows and Secondary Currents in Compound Meandering Channel under the Effect of Building Arrangements

Mohammad Naghavi[1], Mirali Mohammadi[2*], Ghorban Mahtabi[3]

1- PhD in Civil Eng. (Water and Hydraulic Structures), Department of Civil Eng., Urmia University, PO Box 165, Faculty of Eng., Urmia 57561-15311, Iran.

2- Professor in Civil Eng. (Hydraulics and River Eng. Mechanics), Department of Civil Eng., Faculty of Eng., Urmia University, PO Box 165, Urmia 57561-15311, Iran.

3- Associate Professor in Water Eng., Department of Water Eng., University of Zanjan, Zanjan 45371-38791, Iran.

[*] **m.mohammadi@urmia.ac.ir**

Received: 2 November 2023, Accepted: 20 January 2024 J. Hydraul. Homepage: www.jhyd.iha.ir

Abstract

In the present study, flow characteristics in compound meandering channels under the changes of building arrangement in the floodplains were investigated using a numerical simulation. A constant sinuosity factor of 1.21 and relative flow depths (Dr) of 0.29 to 0.49 were considered to illustrate the effect of the hydraulic parameters on the variations of the velocity components. Three types of building arrangements, including structural obstacles perpendicular to the flow of the floodplain (MHT, density=18.5%), structural obstacles parallel to the flow of the floodplain (MGT, density=23.7%), and checkered structural obstacles (MFT, density=23.7%), were used. The simulated data were in good agreement with the experimental data indicating the proper ability of the numerical model in simulation. The result reveals that in the concave arc of sections CS1 and CS7 (apex sections), changing the building arrangements has a negligible effect on the change of transverse and secondary flows due to the parallelism of the main channel flow and the floodplain flow as well as the insignificant effect of the floodplain flow on the main channel. But near the convex arc, these changes are more significant. Hence in section CS4, with the increase of the Dr from 0.29 to 0.49, for cases MAT, MGT, and MHT, the maximum value of depth-averaged transverse flow strength increases by 61%, 91%, and 41%, respectively. In section CS1, the secondary flow cells created in the case of MGT1 cover the entire section; however, in cases of MFT1 and MHT1, the size of the cell is small and is located on the left side of the section. In mid-sections, a small secondary cell in the same direction as the transverse flow (clockwise) is formed in the right corner near the bottom of the channel and gradually grows in the mid-sections and reaches its maximum size in section CS7. Along with the building arrangements of cases MFT1 and MHT1, the transverse component of the floodplain flow velocity (at the entrance of the floodplain flow to the main channel y/h=5) is weakened in the middle sections (CS3, CS4, and CS5). The dimensions of the secondary flow cell increase in the next sections and reach its largest value in section CS7.

Keywords: Compound meandering channel, Building arrangements, Transverse flow, Secondary cell.

1. Introduction

Natural rivers commonly have a meandering main channel and one or two adjacent floodplains well known as compound meandering channels (Knight and Demetriou, 1983). The mechanism of water flows in the compound meandering channels is a 3D complex flow compared with the straight channel (Liu et al., 2014). An extreme exchange of momentum develops between the floodplains and the main channel in a compound meandering channel during flood flows. Therefore, the direction of flow in a floodplain and the main channel is not parallel, so the flow direction in the main channel is parallel to the sidewall of the meandering main channel. Some part of the overbank flow runs downstream along the direction of the floodplain sidewall, and another part enters the meandering main channel to join with the flow of the main channel (Shiono and Muto, 1998). The velocity difference between the main channel flow and floodplain results in forming a shear stress layer between the two areas in the compound meandering channels (Ismail, 2007). Also, due to a large water exchange between the floodplain and the main channel, an additional flow resistance is created (Zhang et al., 2022). In the meandering main channel, secondary currents are formed due to a centrifugal force (Liu et al., 2014). Also, the intense water exchange from the floodplain causes to create a secondary current in the main channel (Shiono and Muto, 1998). Therefore, the secondary flow cells enlarge along the inner bank upstream of the bend and decline rapidly at the transition from the bend to the crossover section. At the outer banks, the vortices rotate in the opposite direction toward that above the outer bank (Shiono and Muto, 1998). Those vortices are eventually moved downstream and significantly enlarge the momentum exchange between the floodplain flows and the main channel, so that the flow structure, erosion, and sedimentation pattern alter significantly in the meandering compound channel (Moncho-Esteve et al., 2018; Pu, 2019, 2022).

In recent decades, numerous experimental research and numerical models have been conducted to study the flow structure and secondary currents in compound meandering channels (Shiono and Muto, 1998; Liu et al., 2014; Moncho-Esteve et al., 2018; Liu et al., 2016). The results of those studies present that the relative depth, roughness, cross-sectional shape and the channel sinuosity are the main factors affecting the flow characteristics in compound meandering channels (Tsujimoto, 1992; Ismail, 2007; Zhang et al., 2021; Mahato et al., 2022). In the natural rivers, roughness in the floodplain areas (e.g. by grasses, canebrakes, verdures, brambles, shrubberies, etc.) influences on the flow structure; increases the flow resistance and decreases the velocity of the flow (Liu et al., 2016; Wang et al., 2020). Some experimental researches were carried out in the compound meandering channels with fixed/mobile bed and floodplain roughness aligns with applications of urban fluvial and hydro-environment systems (Pu et al., 2022). The findings show that the displacement, geometry, and density of roughness have a significant effect on the drag force (Tang et al., 2014; Pu et al., 2016; Kundu et al., 2022).

Ismail (2007) explored the effect of density and arrangement of floodplain vegetation on the flow conditions and sediment transport using laboratory experiments. Multiple secondary current cells are created along the meandering main channel at deeper water depth when the floodplain roughness is enhanced. The secondary cells also cause to significant changes in the bed forms along the meandering channel (Shiono et al., 2009). Shiono et al. (2009) reported the influence of floodplain roughness on the flow characteristics of the main channel and river bedforms. When the roughness of the floodplain surges, several secondary current cells are formed alongside the meandering channel at high depths which results in creating waves in the meandering riverbed. In addition, the direction of rotation of the secondary current cell influences on the riverbed shape. Liu et al. (2016) experimentally studied the effect of floodplain vegetation on the main channel flow structure (Liu et al., 2016). They resented that the transport capacity of the channel significantly reduced due to the roughness, consequently the main channel velocity increases. Also, the intensity of the lateral turbulence in the overbank flow increases and causes to significant variation in the turbulence flow structure.

Variations of the flow velocity distribution in compound meandering channels with one-sided vegetation in floodplains were evaluated (Pan et al., 2019). It was concluded that in the section with maximal density of vegetation in the floodplain, the flow velocity is higher than that

case with minimal density. Near the bending apexes with minimal density, the deflection degrees are smaller than a case with the non-blocked condition in floodplains. While, near the mid-section with a maximal density of vegetation in the floodplain, the deflection degrees are clearly larger than the corresponding values under the smooth floodplain condition. Naghavi et al. (2022,2023a) experimentally examined the behavior of flow in compound meandering channels under the effect of one and two-sided buildings density changes. They concluded that at high relative depth (Dr=0.49), by increasing the two-sided buildings density of the floodplain by 23.7%, the dimensionless longitudinal velocity in the main channel increases by 61%, in comparison with the smooth floodplains. Furthermore, they evaluated the effect of different building arrangements on the flow structures in compound meandering channels was using physical models (Naghavi et al., 2023b). The findings showed that in the arrangement of structural obstacles perpendicular to the floodplain flow, the longitudinal velocity in the main channel increases by 113% compared to the smooth case; but in the case with the arrangement of structural obstacles parallel to the floodplain flow, the flow velocity enhances by only 27%.

Along with the laboratory studies, numerical simulations can present valuable results (e.g., the flow direction and velocity magnitude) about the flow behavior in compound meandering channels and the understanding of turbulent flow characteristics can be developed. High accuracy simulations for the flow characteristics such as the velocity distribution, secondary currents, and depth ratio were reported using several 2D and 3D numerical models (Shiono and Muto 1998; Shukla and Shiono 2008; Moncho-Esteve et al. 2018). Shukla and Shiono (2008) assessed the flow characteristics in the compound meandering channels by computational fluid dynamics (CFD) model. The numerical model has high accuracy in predicting the flow velocity, bed shear stress, water surface level, and turbulent kinetic energy. Sanjou and Nezu (2010) studied the effects of shrubs and trees in floodplain edges on the flow structures. They reported that the streamwise velocity reduces behind trees and near the junction between the main channel and floodplains. A numerical model of turbulent flow in a meandering compound channel was evaluated the results showed that a shear layer is created between the flow in floodplains and the flow throughout the bend when the flow depth increases (Moncho-Esteve et al., 2018). This shear layer generates additional turbulence due to the momentum exchange between the meandering main channel and floodplain flows. Wang et al. (2022) simulated the flow structures in compound meandering channels with presence of the vegetation on the floodplains. With vegetated floodplains, the characteristics of secondary cells change greatly with the increase of Dr. When Dr<0.3, the vortex center of the secondary current moves closer to the outer bank side and the secondary currents distribution shows a pattern dissimilar to flooded condition.

In the last few decades, climate change, population growth on the banks of rivers, and industrialization have resulted in the increasing frequency of occurrence of floods and damages. Thus, it is essential to understand the flooding issues by evaluating the flow structures. However, despite the advancement of knowledge on hydrodynamics, the huge amount of research in laboratory and field conditions as well as by numerical models related to the meandering compound channels, the research about the 3D complex flow characteristics in meandering compound channels with the different buildings located on the floodplains is still rare. In particular, the changes in the secondary flow and the behavior of transverse flows have yet to be studied. The aim of the present research is to numerically investigate the effect of building arrangement changes on the strength of transverse flows and secondary current components in the main channel using a turbulent model.

2. Materials and Methods

2.1. Experimental cases

In this research, the experimental data of Naghavi et al. (2023b) were used. They used a flume with 16 m long, 2.07 m wide, and 0.40 m high (see Figure 1). Different types of building arrangements included the structural obstacles perpendicular to the floodplain flow (MHT, with a density of 18.5%), the structural obstacles parallel to the floodplain flow (MGT, with a density of 23.7%), and the checkered structural obstacles (MFT, with a density of

23.7%). Flow structures of the main channel were evaluated in the cases with different building arrangements at three different relative flow depths. The sinuosity of the main channel (s) was 1.21, the valley slope (S_0) was 0.001, the total width of the channel (B) was 2.07 m, the width of the meandering main channel (b) was 0.5 m and the channel depth (h) was 0.1 m.

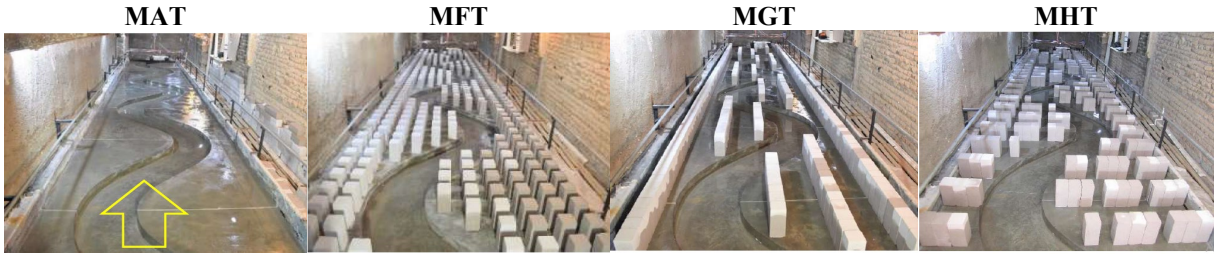

Fig. 1. The laboratory compound meandering channel with different building arrangements (Naghavi et al. 2023b).

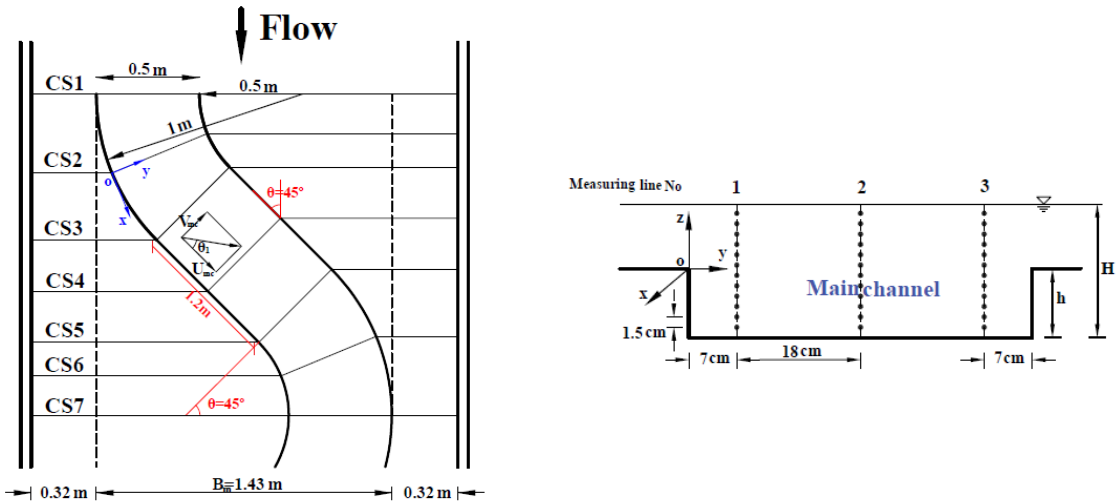

Fig. 2. The plan view and the cross-sectional shape of the channel and measuring sections with the coordinate systems in the main channel.

More details of the experimental conditions and the compound meandering channel geometry used in the experiments and the numerical model are shown in Table 1 and Figure 2, where B_m is the meander belt width, θ is the cross-over angle, θ_1 is the flow angle in the main channel and CS1 to CS7 is the measurement sections for the model meander, Q is the total discharge, H is the flow depth in the main channel, Dr [=(H-h)/H] is the relative flow depth, %St is the percentage of floodplain building density, Fr is the Froude number and Re is the Reynolds number.

Table 1. Experimental parameters (Naghavi et al., 2023)

Case	Q(m^3/s)	H(cm)	Dr	%St	Fr	Re	n
MAT1	0.076	19.5	0.49	0	0.31	30691	0.022
MAT2	0.044	16.4	0.39	0	0.28	18182	0.024
MAT3	0.025	14.1	0.29	0	0.24	10502	0.026
MFT1	0.038	19.5	0.49	23.7	0.16	15528	0.044
MFT2	0.025	16.4	0.39	23.7	0.16	10425	0.041
MFT3	0.016	14.1	0.29	23.7	0.16	6930	0.039
MGT1	0.058	19.5	0.49	23.7	0.24	23415	0.029
MGT2	0.035	16.4	0.39	23.7	0.22	14721	0.029
MGT3	0.019	14.1	0.29	23.7	0.20	8418	0.032
MHT1	0.034	19.5	0.49	18.5	0.14	13943	0.049
MHT2	0.023	16.4	0.39	18.5	0.15	9591	0.045
MHT3	0.014	14.1	0.29	18.5	0.14	6122	0.044

2.2. Numerical models and governing equations

A CFD model was provided to study the transverse flows and secondary currents in compound meandering channels under the variations of building arrangement. Data of the experimental models of Naghavi et al. (2023b) were used for the validation of the numerical model. Herein, to simulate the flow behavior in the meandering compound channel, Flow-3D software was used. Flow-3D is capable to solve complex fluid dynamics problems and user friendly as well as has a very powerful graphical interface that makes it easier to work with. In this software, Finite Volume Method is used to solve governing equations and using regular networking and volume of fluid methods to calculate free surface level in open channels. Flow-3D software governs by Navier-Stokes momentum and continuity equations for the entire computing space. The governing continuity equation and the Reynolds-Averaged Navier–Stokes (RANS) equations are:

$$V_f \frac{\partial \rho}{\partial t} + \frac{\partial(\rho u A_x)}{\partial x} + \frac{\partial(\rho v A_y)}{\partial y} + \frac{\partial(\rho w A_z)}{\partial z} = R_{SOR} \quad (1)$$

$$\frac{\partial u}{\partial t} + \frac{1}{V_f}\left(u A_x \frac{\partial u}{\partial x} + v A_y \frac{\partial u}{\partial y} + w A_z \frac{\partial u}{\partial z}\right) = -\frac{1}{\rho}\frac{\partial P}{\partial x} + G_x + f_x \quad (2)$$

$$\frac{\partial v}{\partial t} + \frac{1}{V_f}\left(u A_x \frac{\partial v}{\partial x} + v A_y \frac{\partial v}{\partial y} + w A_z \frac{\partial v}{\partial z}\right) = -\frac{1}{\rho}\frac{\partial P}{\partial y} + G_y + f_y \quad (3)$$

$$\frac{\partial w}{\partial t} + \frac{1}{V_f}\left(u A_x \frac{\partial w}{\partial x} + v A_y \frac{\partial w}{\partial y} + w A_z \frac{\partial w}{\partial z}\right) = -\frac{1}{\rho}\frac{\partial P}{\partial w} + G_z + f_z \quad (4)$$

where, (u, v, w) are velocity components; (A_x, A_y, A_z) are flow area fractions; (G_x, G_y, G_z) are mass accelerations; and (f_x, f_y, f_z) are viscous accelerations in (x, y, z) directions, ρ is the fluid density, R_{SOR} is the spring term, V_f is the fraction of the volume associated with the flow, and P is the pressure. In this study, the flow turbulence was represented by solving the RANS equations using the Reynolds Renormalization Group (RNG) turbulent model. Naghavi et al. (2019, 2023c, 2024) showed that the RNG turbulent model has high accuracy in simulating the flow in meandering compound channels. Literature reviews of numerical studies presented that the RNG model can accurately predict the Reynolds shear stress and can generate secondary currents properly (Pu et al. 2014; Pu 2015). The equations of the RNG turbulent model are as follows (Yakhot et al. 1992):

$$\frac{\partial k}{\partial t} + \bar{u}_i \frac{\partial k}{\partial x_i} = \nu_t \ S^2 - \epsilon + \frac{\partial}{\partial x_i}\left(\alpha \ \nu_t \frac{\partial k}{\partial x_i}\right) \quad (5)$$

$$\frac{\partial \epsilon}{\partial t} + \bar{u}_i \frac{\partial \epsilon}{\partial x_i} = C_{\epsilon 1} \frac{\epsilon}{k} \ \nu_t \ S^2 - C_{\epsilon 2} \frac{\epsilon^2}{k} - R + \frac{\partial}{\partial x_i}\left(\alpha \ \nu_t \frac{\partial \epsilon}{\partial x_i}\right) \quad (6)$$

where, k is the turbulent kinetic energy, ϵ the dissipation rate, ν_t the turbulent eddy viscosity, S^2 the magnitude of the strain rate, $R = \frac{C_\mu \eta^3 (1-\eta/\eta_0)}{1+\beta \eta^3}\frac{\epsilon^2}{k}$, $\eta = \frac{Sk}{\epsilon}$. Coefficients of C_μ $C_{\epsilon 1}$, $C_{\epsilon 2}$, η_0, α, and β are constants, and their values are listed in Table 2. For tracking and locating the free surface flow, the volume of fluid (VOF) method was used. This technique belongs to the class of Eulerian method based on the idea of a fraction function, $F(x, y, z, t)$, indicating the ratio of the volume occupied by the fluid to the total volume of a grid. Three considered cases were: (*i*) a cell is empty without traced fluid inside, the value of function F=0; (*ii*) the cell is full, F=1; and (*iii*) there is a fluid interface in the cell, 0<F<1.

Table 2. Coefficients for the RNG turbulent model (Yakhot et al. 1992).

C_μ	$C_{\epsilon 1}$	$C_{\epsilon 2}$	η_0	α	β
0.085	1.42	1.68	4.38	1.39	0.012

2.3. Boundary conditions and model gridding

Figure 3 shows the numerical models of the different building arrangements based on the physical model used in Naghavi et al. (2023). The boundary conditions of the numerical model are the same as the physical model. The volume flow rate and specified pressure

boundary conditions were defined at the entrance and exit of the meandering compound channel, respectively. Wall boundary conditions were used for the bed and sidewalls of the channel. For the free surface, a symmetry boundary condition was applied (Moncho-Esteve et al. 2018). Figure 4 shows the boundary conditions of the flow domain. The FLOW-3D model employs cubic cells (regular grids). To obtain accurate results, the optimal grid spacing was determined by checking mesh quality based on the adjacent cell size ratio and the aspect ratio. The optimal ratios are close to 1. The maximum of adjacent cell size ratio and the aspect ratio do not exceed 1.25 and 3, respectively. Consequently, the meshes were re-adjusted so that the limits of the ratios were satisfied. Furthermore, the grid was refined to reduce errors in the numerical model (Table 3). It was found that the model with very fine grids has a lower mean absolute percentage error (MAPE, %) than the other models. In addition, results obtained by fine grids are very similar to those by very fine grids. Grid-independent results suggested that fine grids ensure reasonable accuracy, so this grid was used for all simulations. The grid resolution determining method used here is similar to those in the literature (Moncho-Esteve et al. 2018; Pu 2015; Xu et al. 2013; Van et al. 2014; Brevis et al. 2014). The MAPE (%) and the root mean square error (RMSE) for each quantity are calculated by equations (7) and (8) as follows:

$$MAPE = 100 \times \frac{1}{n}\sum_{i=1}^{n}\left|\frac{E_i - N_i}{E_i}\right| \quad (7)$$

$$RMSE = \sqrt{\frac{1}{n}\sum_{i=1}^{n}(E_i - N_i)^2} \quad (8)$$

where, E_i is the value of experimental data, N_i is the value of numerical data, and n is a number of data.

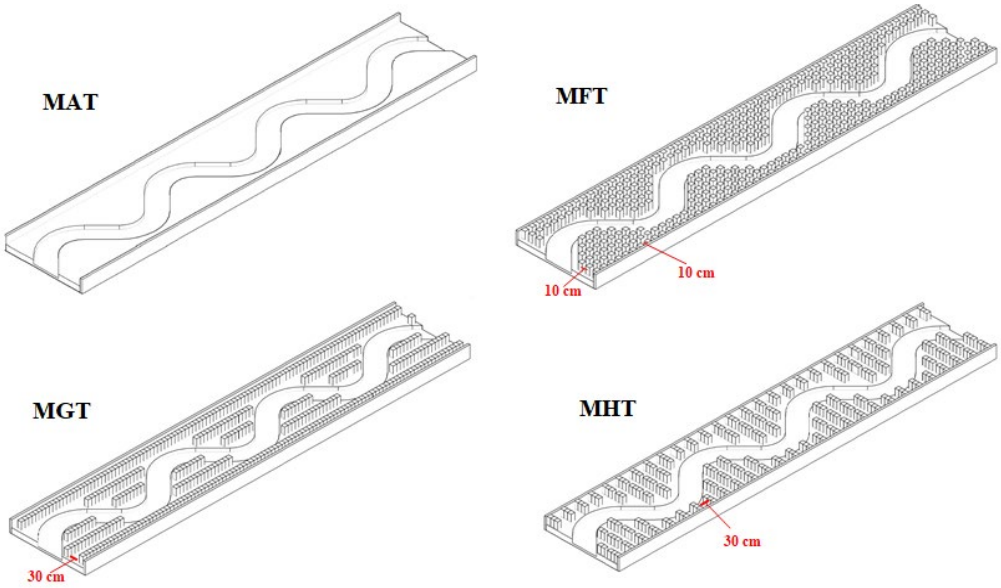

Fig. 3. Numerical models created for different building arrangements.

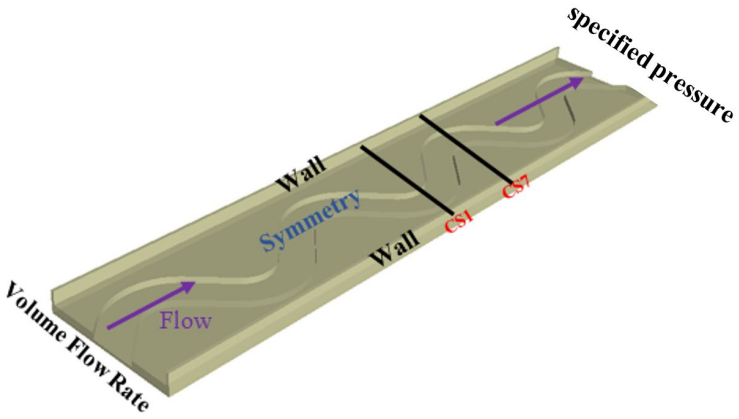

Fig. 4. Boundary conditions for the flow domain.

Table 3. The accuracy of different model grids based on the mean absolute percentage error (MAPE,%) of depth-averaged velocities calculated in sections CS1 and CS4 for cases MAT1, MFT1, MGT1 and MHT1.

Type of gridding	Grid spacing (cm)	MAPE (%)							
		MAT1		MFT1		MGT1		MHT1	
		CS1	CS4	CS1	CS4	CS1	CS4	CS1	CS4
Coarse	3	8.82%	9.17%	9.86%	10.24%	10.11%	10.66%	10.89%	11.26%
Medium	1.5	5.93%	6.21%	6.84%	7.16%	7.09%	7.46%	7.73%	7.95%
Fine	1	3.55%	3.96%	4.45%	4.96%	4.54%	4.99%	5.04%	5.22%
Very Fine	0.75	3.53%	3.94%	4.42%	4.93%	4.51%	4.95%	5.01%	5.18%

2.4. Model validation

To validate the results of numerical model, the values of Q_{mc}/Q (the ratio of main channel discharge to the total discharge), depth-averaged velocity and longitudinal flow velocity in different sections of the main channel were compared with the experimental model results of Naghavi et al. (2023). Figures 5 and 6 show the comparison of the experimental and numerical results of Qmc/Q in sections CS1-CS7 at Dr=0.29 and depth-averaged velocities in section CS4 at Dr= 0.29, respectively, for cases with different building arrangements. The results show that the calculated Qmc/Q and depth-averaged velocities are in reasonable agreement with the experimental data measured for all cases. Figure 7 shows a comparison of experimental and numerical results for longitudinal flow velocity (U) in cases MAT1 and MFT1 and

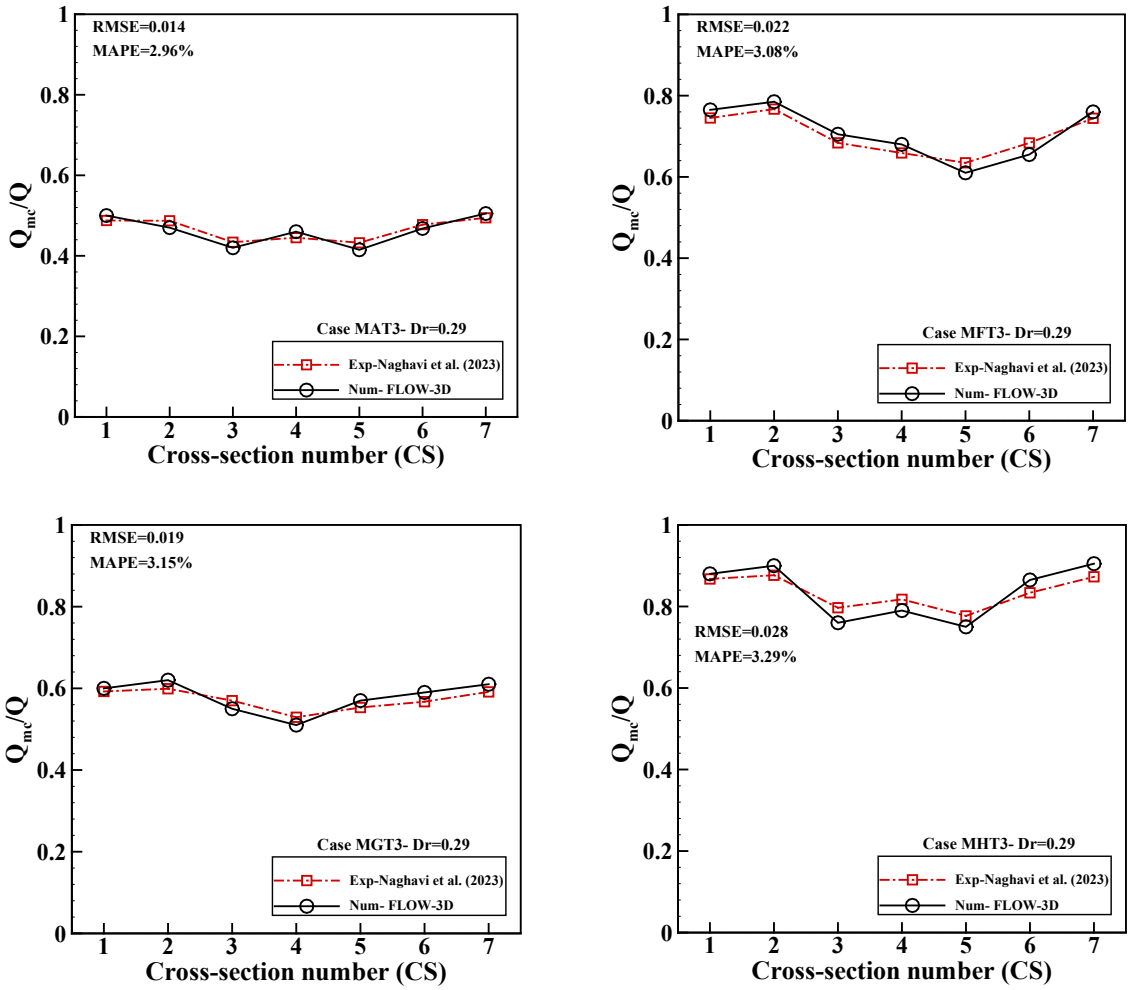

Fig. 5. A comparison of experimental and numerical results for Q_{mc}/Q in relative depth of 0.29.

sections CS4 and CS7. The simulated velocity profile reproduces the corresponding results to the experimental data. The MAPE error values also reconfirm the good agreement between the numerical and experimental results (see Table 3). De Marchis and Napoli (2008) and Xu et al. (2013) numerically computed the complex properties of three-dimensional flows in meandering compound channels, and they showed similar discrepancies of their simulations to actual measurements in most compared cases.

3. Results and Discussion

3.1. Secondary flow cells in the main channel

In Figures 8 to 12, the process of growth and decay of secondary flow cells at different sections of the main channel for different building arrangements are presented in vector form. According to Figure 8, in section CS1, the secondary flow cell created in cases MAT1 and MGT1 covers the entire section; but in cases MFT1 and MHT1, the size of the cell is smaller, and located only at the left half of the section. In cases MAT1 and MGT1, the center of the secondary flow cell is about y/h=2, but in cases MFT1 and MHT1, their centers of the secondary flow cell are y/h=1.6 and y/h=1.4, respectively.

For cases, MAT1 and MGT1, the center of the secondary flow cell occurs near the bankfull level, but in cases MFT1 and MHT1, the cell center is above the bankfull level. In sections CS1 and CS7, near the convex arc, the strength of the secondary flow in cases MFT1 and MHT1 is higher than in cases MAT1 and MGT1. At these sections, by changing the building arrangement, the flow velocity in the main channel changes and so as the centrifugal force. Consequently, stronger secondary flows are created for those cases. In section CS2, the secondary flow cell disappears in cases for different building arrangements, and the transverse flow spreads over the entire section. In sections CS3, CS4, and CS5, due to the increase in the deviation angle of the main

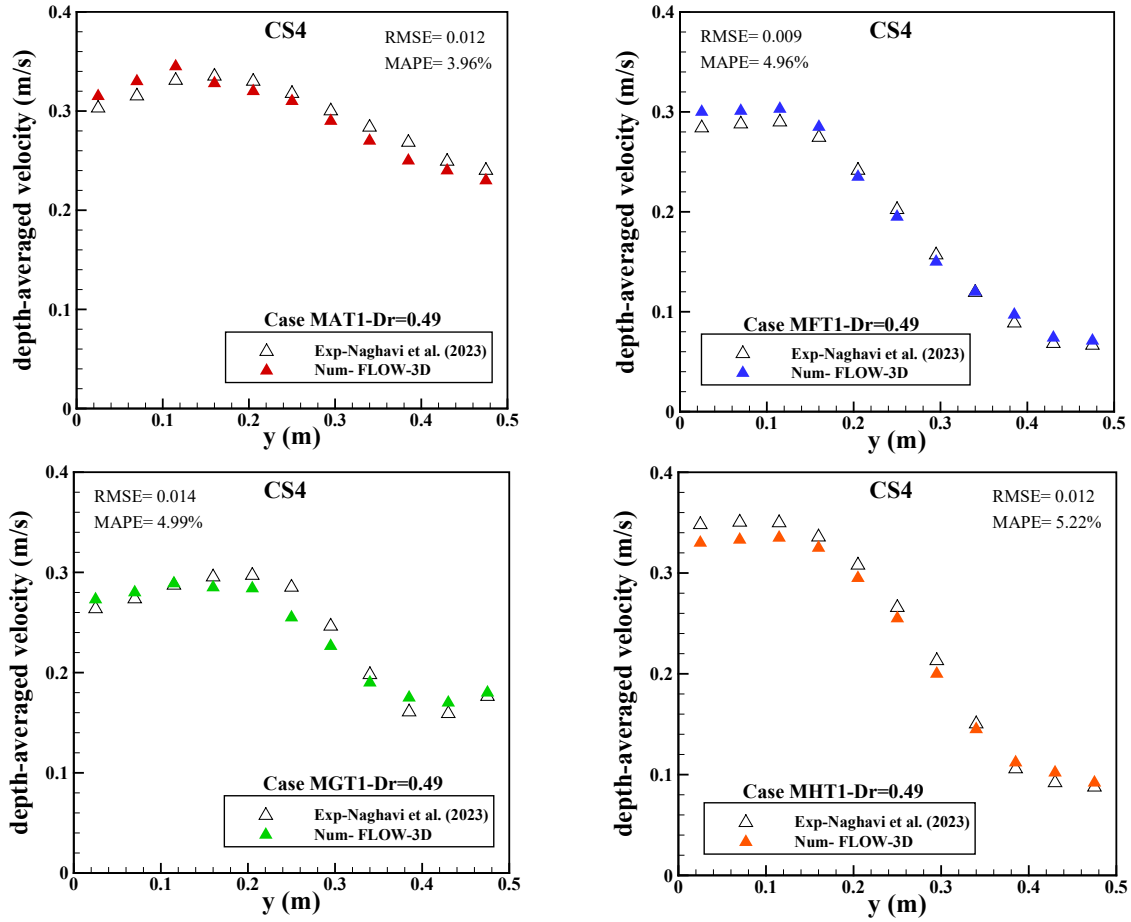

Fig. 6. A comparison of experimental and numerical results for depth-averaged velocities in section CS4 and relative depth of 0.49.

channel compared to the floodplain for cases MAT1 and MGT1, transverse flows with greater strength enter the main channel from the floodplain, and as a consequence, a small secondary flow cell in the same direction as the transverse flow (clockwise) is formed in the right corner near the bottom of the channel in section CS3 and gradually grows in CS4, CS5, CS6 and reaches its maximum size in CS7. Along with the building arrangements of cases MFT1 and MHT1, the transverse component of the floodplain flow velocity (at the entrance of the floodplain flow to the main channel y/h=5) is weakened in the middle sections (CS3, CS4, and CS5). This causes the transverse flow and secondary flow cell created in the right corner of the main channel (y/h=5) to be very small. The dimensions of the secondary flow cell increase in the next sections and reach its largest value in section CS7. As can be seen in Figures 8 and 11, near the convex arc in section CS1, the secondary flow strength in cases MFT1 and MHT1 is higher than MAT1 and MGT1; and on the other hand, in section CS4, the secondary flow strength in cases MFT1 and MHT1 is weaker than that of MAT1 and MGT1. The centrifugal force is dominant in section CS1, but the transverse flow of the floodplain is dominant in the section CS4. In section CS1, according to the building arrangements of MFT1 and MHT1, the floodplain flow velocity decreases and the majority of the flow discharge passes through the main channel. The flow velocity in the main channel increases, and as a reaction, the centrifugal force and transverse flow increase. In section CS4 (with the building arrangements of MFT1 and MHT1), the floodplain flow velocity decreases (the arrangement of obstacles in the floodplain is such that it prevents the entrance of floodplain flow to the main channel), and as a result, the contribution of floodplain flow in the production of the secondary flow of the main channel decreases.

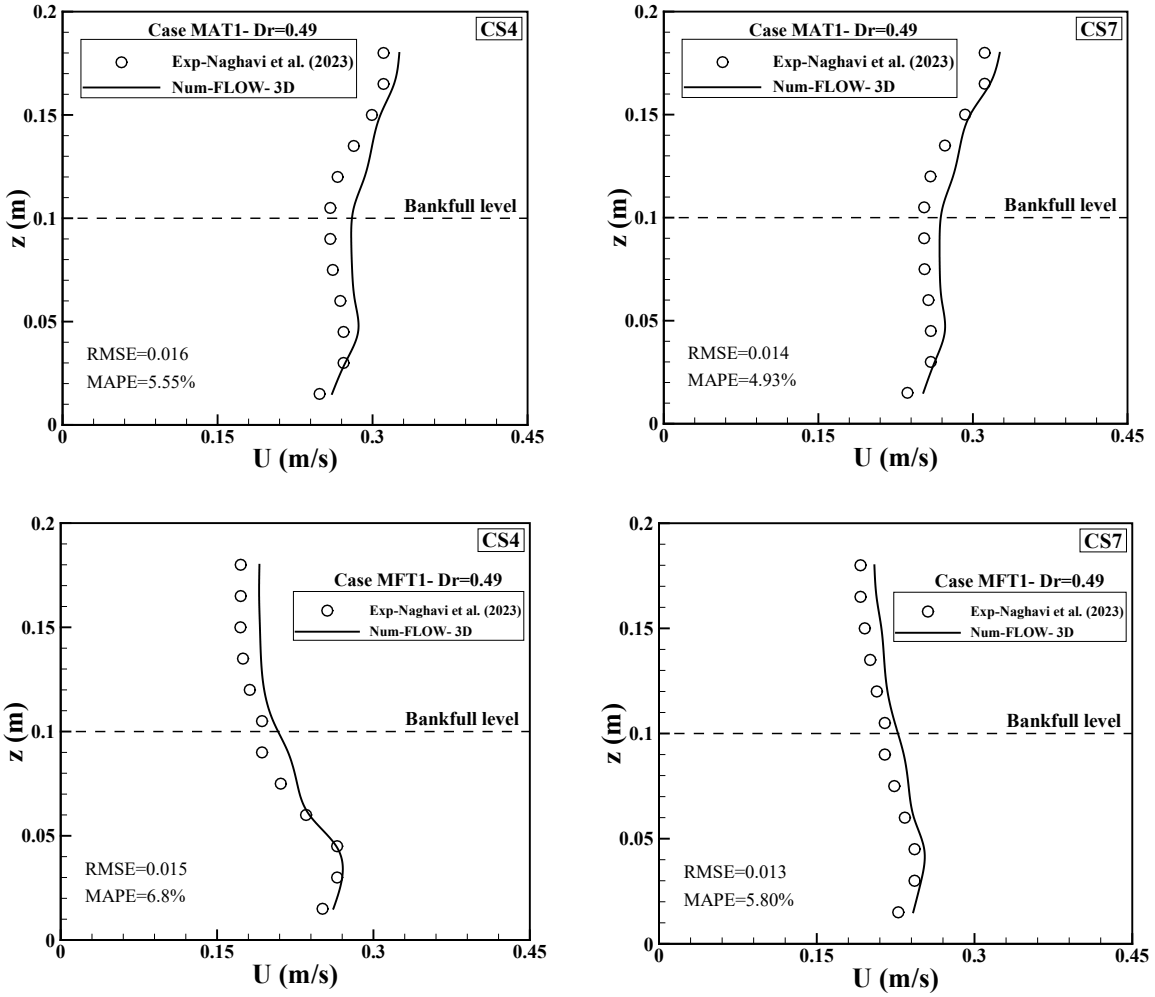

Fig. 7. A comparison of experimental and numerical results for longitudinal flow velocity (U) in cases MAT1 and MFT1 and sections CS4 and CS7.

3.2. The strength of transverse flows

In this section, the equations of Shukry (1950) were used to calculate the strength of transverse flows in meandering compound channel under the effect of changing the building arrangement. Shukry (1950) used the ratio of the kinetic energy of the lateral flow to the kinetic energy of the main flow, therefore, the strength of the transverse flows is calculated as:

$$S_{yz} = \frac{K_{lateral}}{K_{main}} = (\frac{V^2{}_{yz}}{2g})/(\frac{V^2}{2g}) = \frac{(v^2+w^2)}{(u^2+v^2+w^2)}$$

Figure 15 presents the strength of the transverse flows along flow depth (z) with distances of 0.07, 0.25 and 0.43 meters from the left wall of the main channel at a relative depth of 0.49. The results show that the change of building arrangement in sections CS1 and CS7 has negligible impact on the transverse flow strength; but in the middle sections (CS3-CS5), due to the increase in the deviation angle of the main channel, the effect of the transverse flow of the floodplain is significant. The placement of structural barriers has a great effect on the strength of the transverse flow, where in the

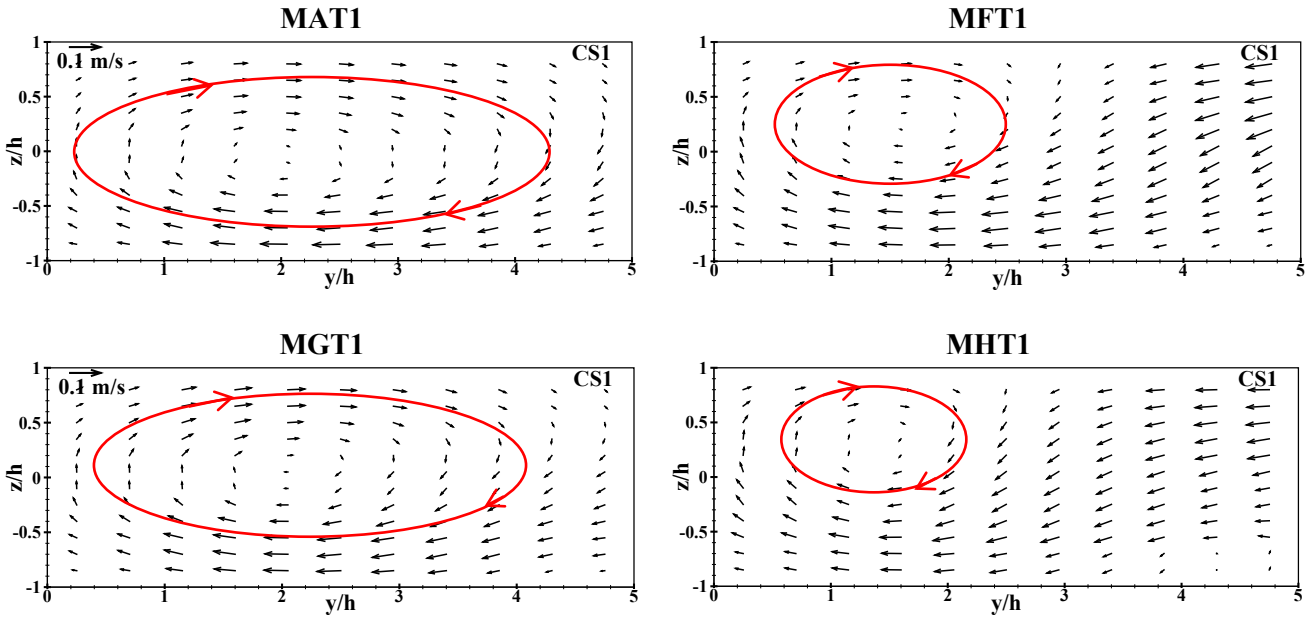

Fig. 8. Secondary flow distribution in section CS1 for different building arrangements.

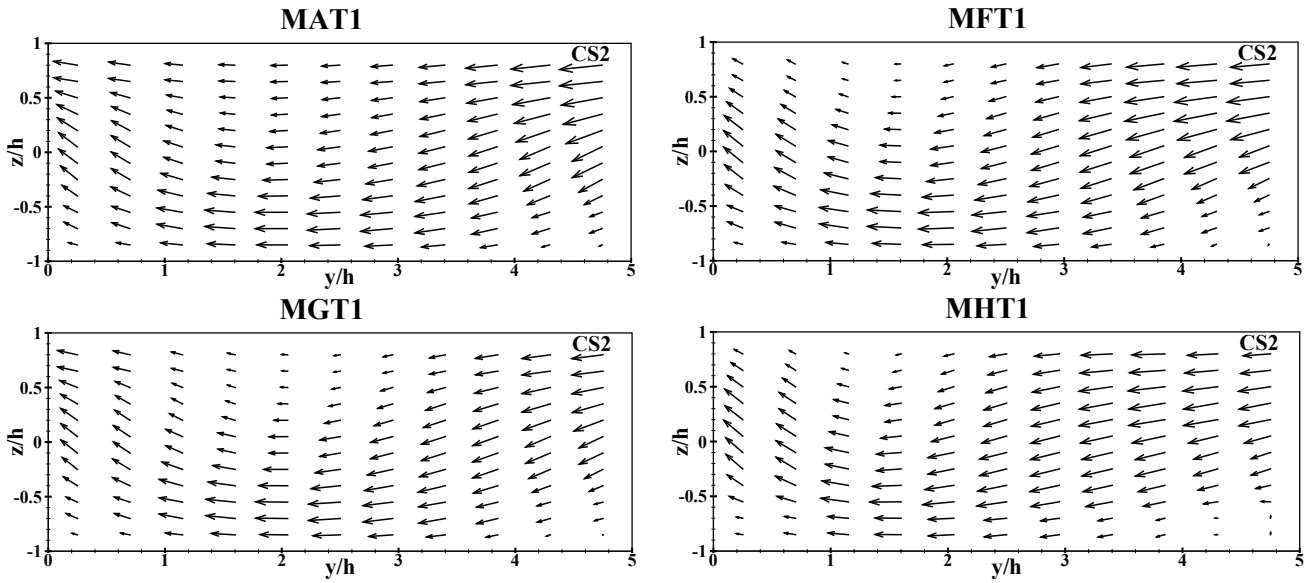

Fig. 9. Secondary flow distribution in section CS2 for different building arrangements.

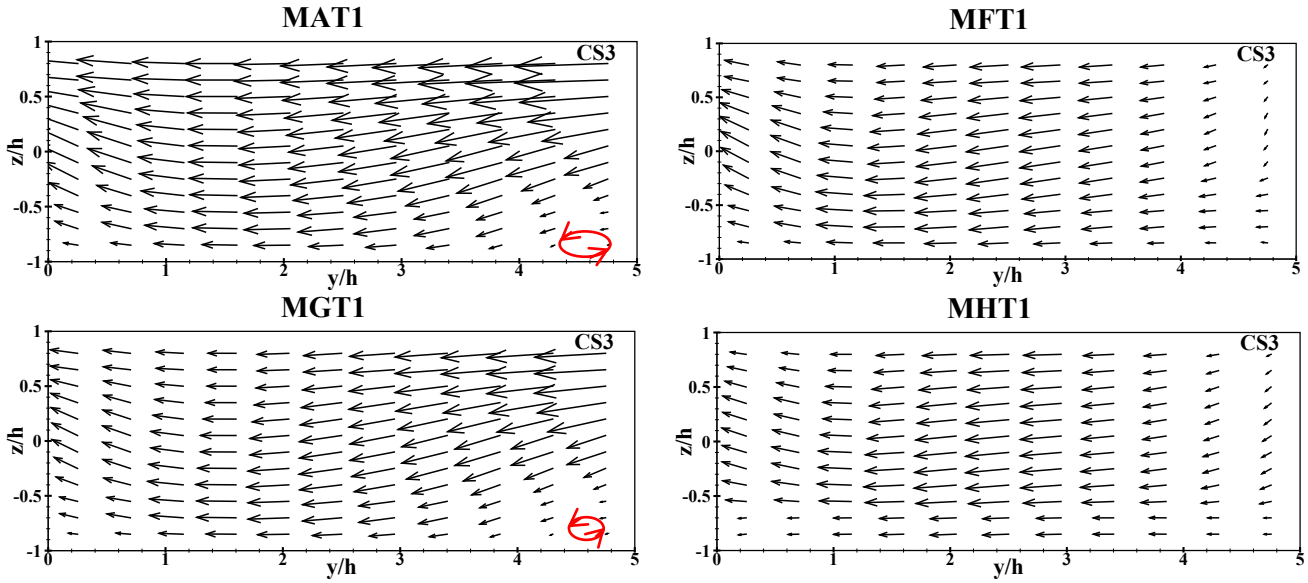

Fig. 10. Secondary flow distribution in section CS3 for different building arrangements.

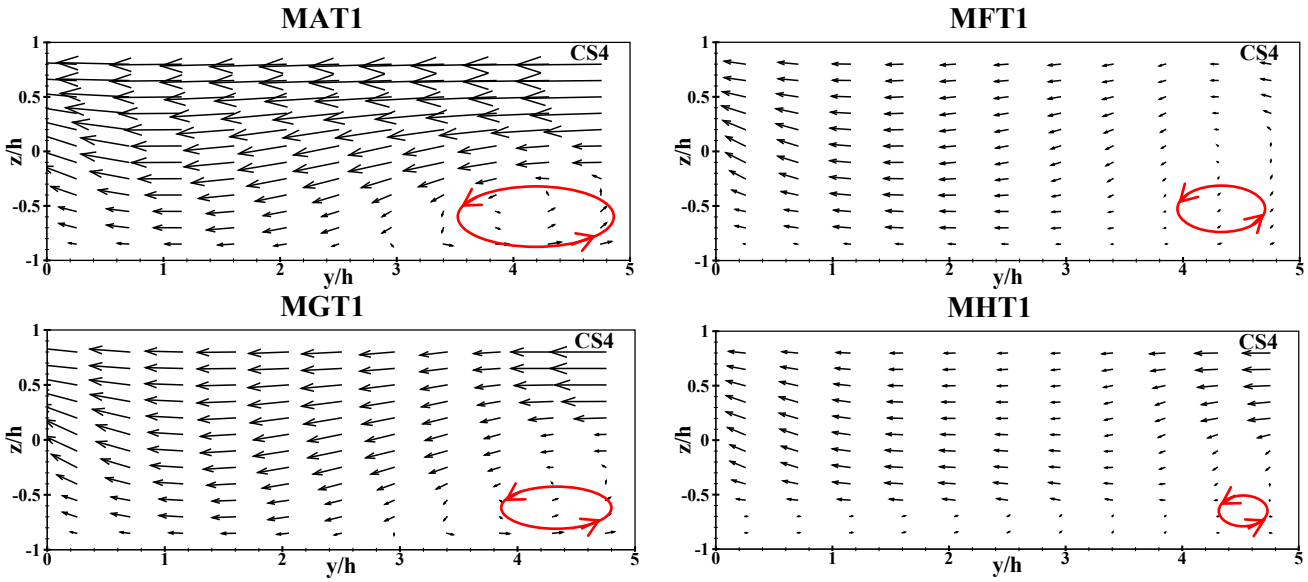

Figure 11. The location and magnitude of secondary flow cell in section CS4 for different building arrangements.

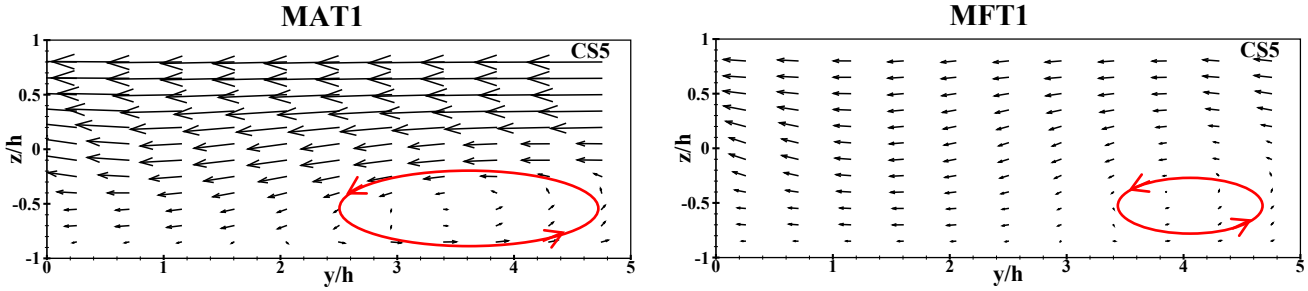

Fig. 12. Secondary flow distribution in section CS5 for different building arrangements.

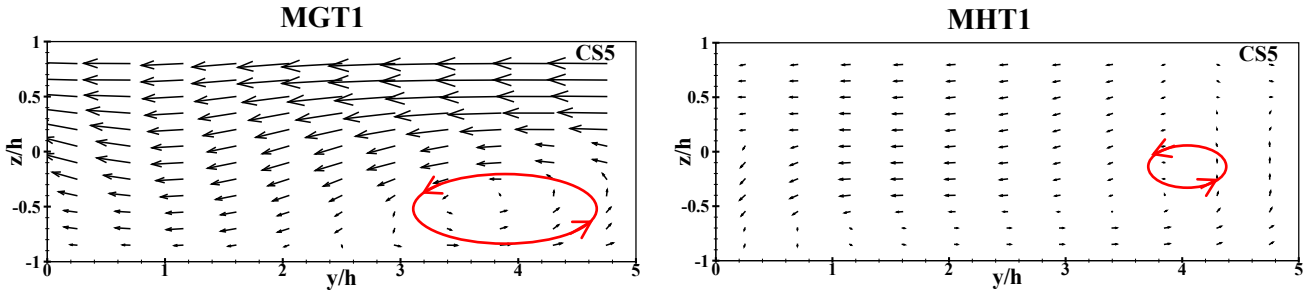

Fig. 12. Continued.

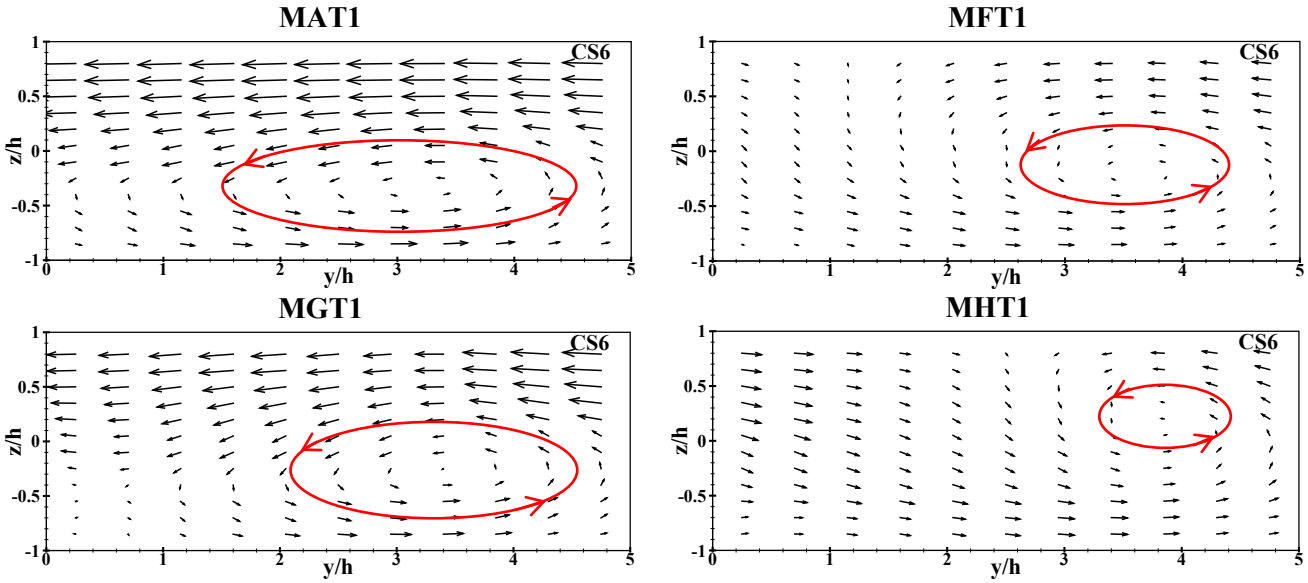

Fig. 13. Secondary flow distribution in section CS6 for different building arrangements.

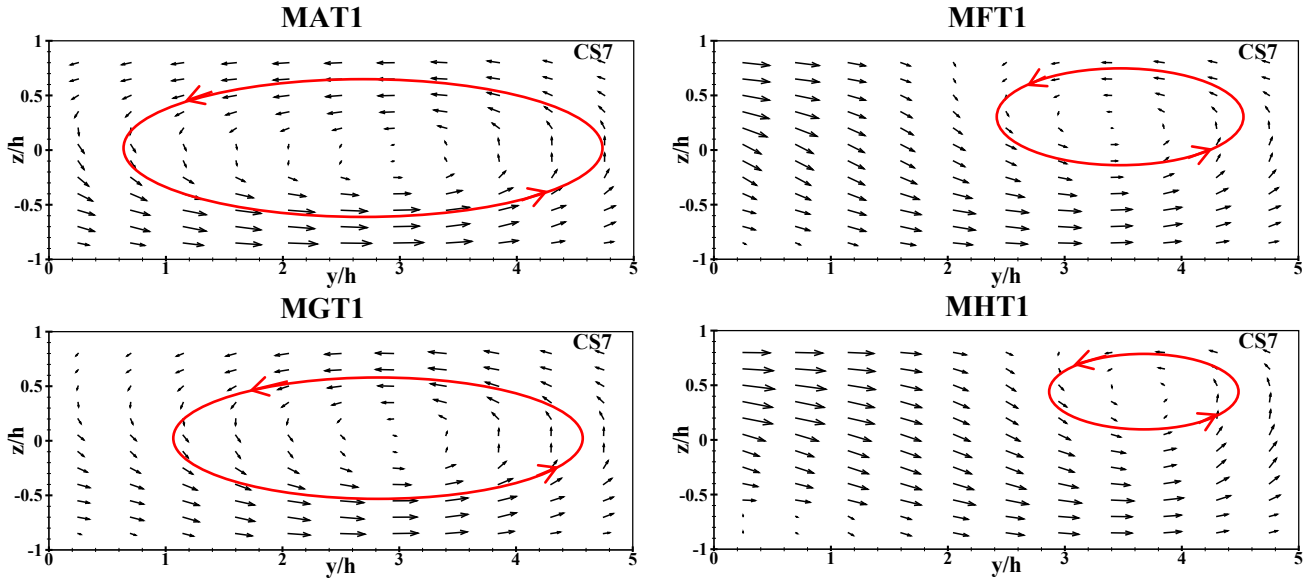

Fig. 14. Secondary flow distribution in section CS7 for different building arrangements.

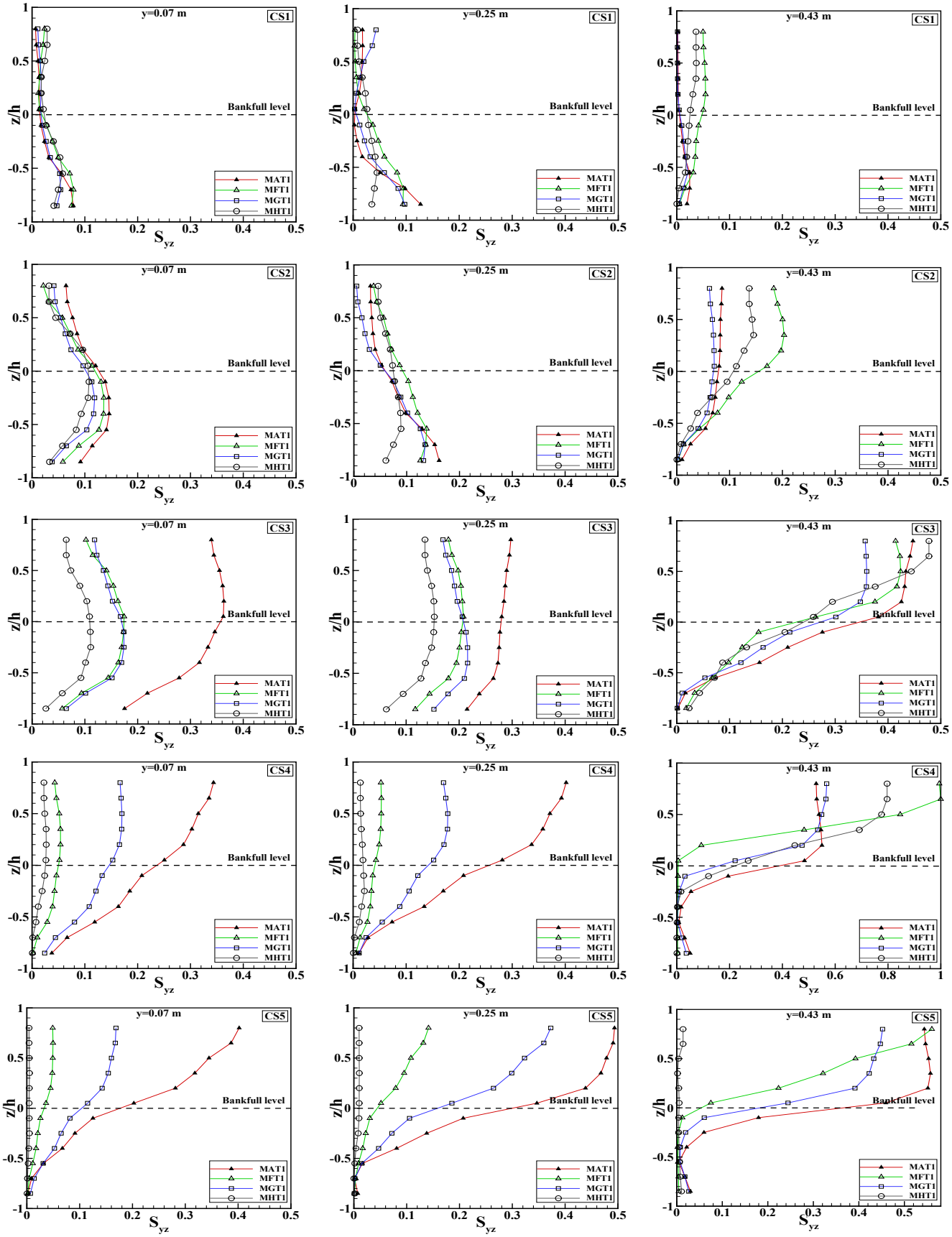

Fig. 15. Variations of transverse flow strength in the direction of flow depth (z) at three axes for different building arrangements.

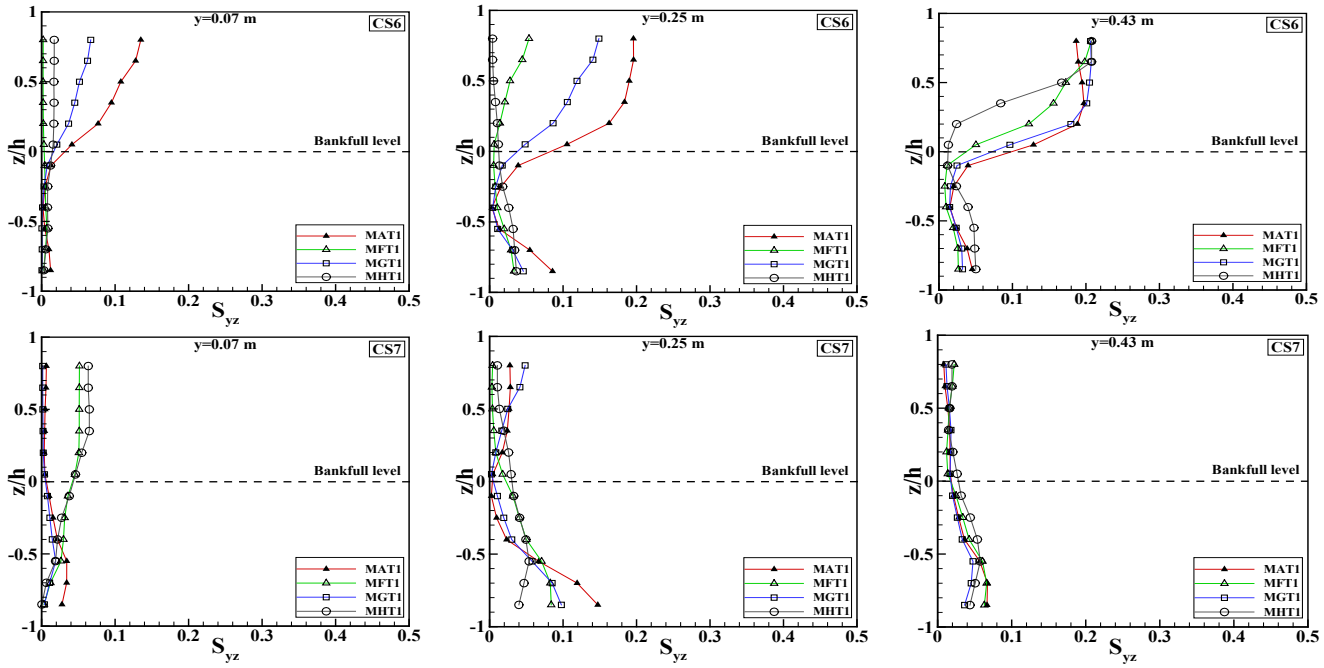

Fig. 15. Continued.

MGT1 channel, the transverse flow strength is higher than in the MHT1 channel. The arrangement of structural barriers in case MGT1 is such that it easily transfers the floodplain flow, but in case MHT1, due to the arrangement that is perpendicular to the direction of the floodplain flow, the intensity of the transverse floodplain flow is significantly reduced. These changes are more noticeable at the place where the flow exits from the main channel to the floodplain (near the left wall, y=0.07 m), in which for MFT1 and MHT1 with the most structural obstacles, the lowest amount of transverse flow was shown. In sections CS3-CS5, the changes in the transverse flow strength at the z depth are large due to the increase in the intensity of the transverse floodplain flow, where the maximum value is observed above the bankfull level and the minimum value is observed below the bankfull level.

Figure 16 shows the depth-averaged transverse flow strength for different building arrangements at relative depth of 0.49. In the middle sections (CS3-CS5), the depth-averaged transverse flow strength in case MAT (without any structural barriers in the floodplain) is higher than other building arrangements. In case MAT, the transverse flow of the floodplain enters the main channel with greater intensity due to the absence of structural barriers in the floodplain. As a result, the transverse flow velocity (v) in the main channel and transverse flow strength are high (compared to other building arrangements). Due to the type of building arrangement and the resistance created against the flow entering the main channel in case MHT (with a structural arrangement perpendicular to the direction of the floodplain), the transverse flow strength has the lowest value. In sections CS1 and CS7, the building arrangement change has a negligible effect on the transverse flow strength due to the parallelism of the main channel flow and the floodplain flow as well as the insignificant effect of the floodplain flow on the main channel.

In Figure 17, depth-averaged transverse flow strength for building arrangements at different relative depths is shown. According to this figure, in the middle sections (CS3, CS4 and CS5) with the increase of the relative depth, the amount of transverse flow strength increases. As a consequence, in section CS4, with the increase of the relative depth from 0.29 to 0.49, for cases MAT, MGT and MHT, the maximum value of depth-averaged transverse flow strength increases by 61%, 91%, and 41%, respectively. According to Figure 17, in sections CS1 and CS7, the change in relative depth has a negligible effect on the transverse flow strength, and these changes are more noticeable in the middle sections.

4. Conclusions

In the present research work, the behavior of transverse flows, and secondary currents in

meandering compound channels under the effect of changing building arrangement was investigated. For this purpose, three different building arrangements have been used, and the results have also been compared with smooth floodplains. Measurements were acquired in

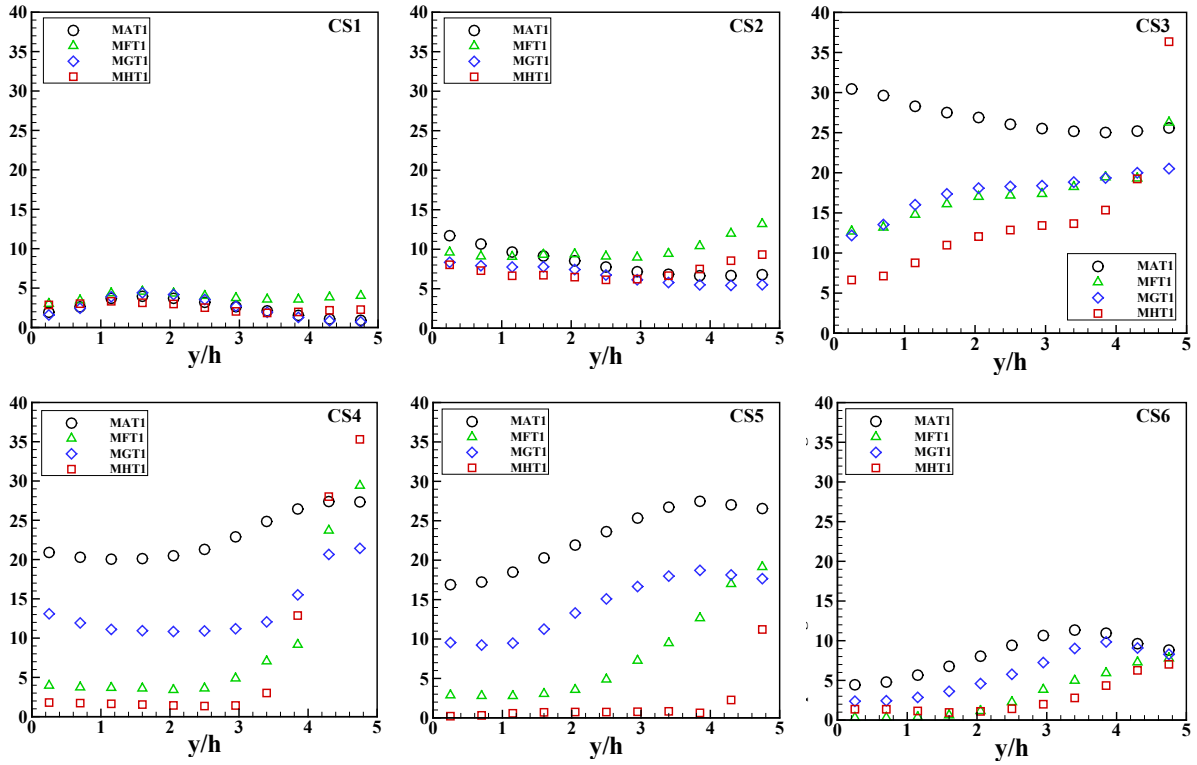

Fig. 16. Depth-averaged transverse flow strength for different sections at a relative depth of 0.49.

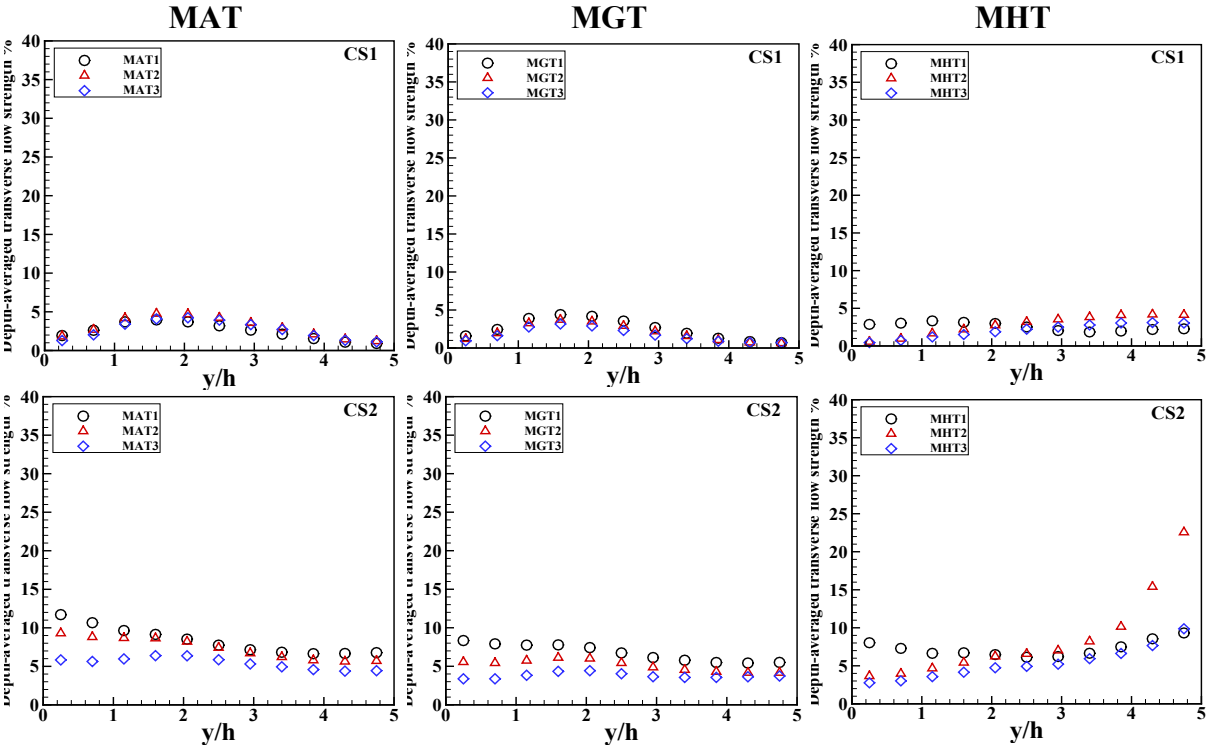

Fig. 17. Depth-averaged transverse flow strength for different relative depth.

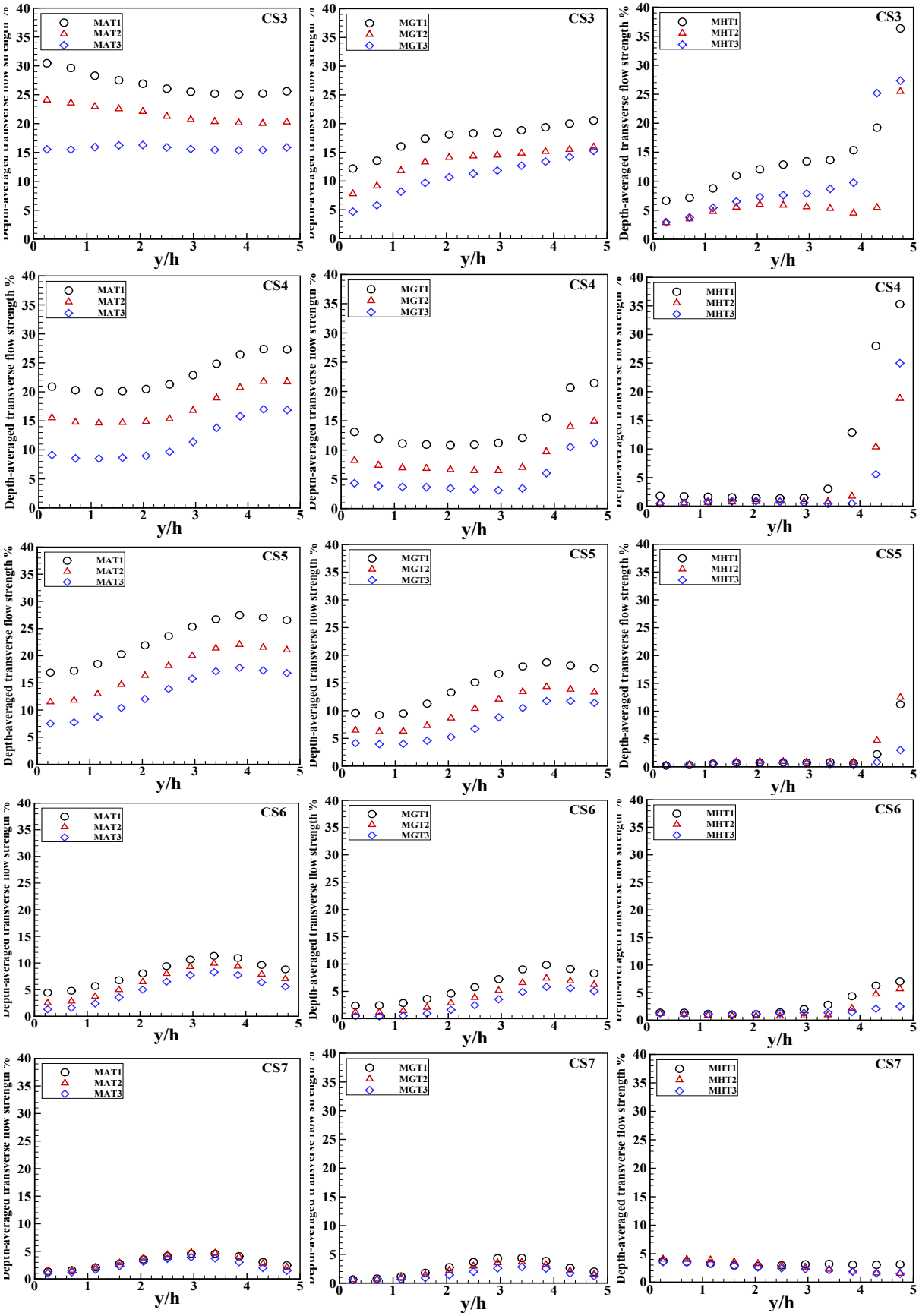

Fig. 17. Continued.

seven sections along the meandering main channel for different relative depths. The findings of this paper will help the researchers to understand the effects of building

arrangements on flow behavior due to transverse flow in a meandering main channel. According to the comparison between the results of this research and previous studies, it was indicated that the buildings built in the floodplain of meandering compound channels increase the flow resistance and decrease the flow through the floodplain, so the amount of flow through the main channel increases. As a result, the cell size of the secondary currents in the main channel decreases with the increase in flow resistance in floodplain.

The main conclusions are drawn as:

1- In apex sections (CS1 and CS7), the secondary flow cell created in cases MAT1 and MGT1 covers the entire section, but in cases MFT1 and MHT1, the size of the cell is smaller and it is located in the concave arc of sections CS1 and CS7.
2- In section CS1, the secondary flow strength in cases MFT1 and MHT1 is higher than MAT1 and MGT1 near the convex arc; on the other hand, in section CS4, the secondary flow strength in cases MFT1 and MHT1 is weaker than MAT1 and MGT1. In section CS1, the centrifugal force is dominant; but in section CS4, the transverse flow of floodplain is dominant.
3- The change of building arrangement has a negligible effect on the transverse flow strength in sections CS1 and CS7, but in the middle sections (CS3, CS4 and CS5), this effect to floodplain flow is significant. The placement of structural barriers has a great effect on the strength of the transverse flow, therefore in the MGT1 channel, the transverse flow strength is observed more than in the MHT1 channel.
4- In apex sections (CS1 and CS7), the change in relative depth has a negligible effect on the transverse flow strength, and these changes are more noticeable in the middle sections, hence in section CS4, with the increase of the relative depth from 0.29 to 0.49, for cases MAT, MGT and MHT, the maximum value of depth-averaged transverse flow strength increases by 61%, 91% and 41%, respectively.

5. References

Brevis, W., García-Villalba, M. & Niño, Y. (2014). Experimental and large eddy simulation study of the flow developed by a sequence of lateral obstacles. *Environmental Fluid Mechanics*. *14*, 873–893.

De Marchis, M. & Napoli, E. (2008). The effect of geometrical parameters on the discharge capacity of meandering compound channels. *Advances in Water Resources*. *31*, 1662–1673.

Ismail, Z. (2007). A study of overbank flows in non-vegetated and vegetated floodplains in compound meandering channels. Dissertation for the Doctoral Degree. Loughborough :University of Loughborough.

Knight, D.W. & Demetriou, J.D. (1983). Floodplain and main channel flow interaction. *Journal of Hydraulic Engineering*. *109*(8), 1073–1092.

Kundu, S., Chattopadhyay, T. & Pu, J.H. (2022). Analytical models of mean secondary velocities and stream functions under different bed-roughness configurations in wide open-channel turbulent flows. *Environmental Fluid Mechanics*. *22*(1), 159-188.

Liu, C., Wright, N., Liu, X. & Yang. K. (2014). An analytical model for lateral depth-averaged velocity distributions along a meander in curved compound channels. *Advances in Water Resources*. *74*, 26-43.

Liu, C., Shan, Y., Liu, X., Yang, K. & Liao, H. (2016). The effect of floodplain grass on the flow characteristics of meandering compound channels. *Journal of Hydrology*. *542*, 1-17.

Mahato, R.K., Dey, S. & Ali, S.Z. (2022). Planform evolution of a sinuous channel triggered by curvature and autogenic width oscillations due to generic grain transport. *Physics of Fluids*. *34*(4), 044110, https://doi.org/10.1063/5.0087971.

Moncho-Esteve, I., Palau-Salvador, G., García-Villalba, M., Muto, Y. & Shiono, K. (2018). A numerical study of the complex flow structure in a compound meandering channel. *Advances in Water Resources*, *116*, 95–116.

Naghavi, M., Mohammadi, M.A. & Mahtabi, G. (2019). Flow Velocity in Meandering Compound Channel under the Influence of Sinusoidal Change. *Modares Civil Engineering journal*, *19*(5), 208-219.

Naghavi, M., Mohammadi, M. & Mahtabi, G. (2020). Turbulence Intensity and Boundary Shear Stress in Meandering Compound Channel under the Influence of Sinusoidal Changes. *Journal of Modeling in Engineering*, *18*(60), 53-69.

Naghavi, M., Mohammadi, M. & Mahtabi, G. (2021). Numerical simulation of flow velocity distribution and shear stress in meandering compound channels. *Iranian Water Researches Journal*, *15*(1), 23-34.

Naghavi, M., Mohammadi, M. & Mahtabi, G. (2021). Transverse Flow Characteristics in the Meandering Compound Channels. *Amirkabir Journal of Civil Engineering*, *53*(8), 3499-3516.

Naghavi, M., Mohammadi, M. & Mahtabi, G. (2021). On the effect of relative flood depth on flow hydraulics in meandering compound channels. *Irrigation and Water Engineering*, *11*(3), 55-78.

Naghavi, M., Mohammadi, M. & Mahtabi, G. (2022). An experimental evaluation of the blocks in floodplain on hydraulic characteristics of flow in a meandering compound channel. *Journal of Hydrology*, *612*, 127976, https://doi.org/10.1016 /j.jhydrol.2022.127976.

Naghavi, M., Mohammadi, M., Mahtabi, G. & Abraham, J. (2023a). Experimental assessment of velocity and bed shear stress in the main channel of a meandering compound channel with one-sided blocks in floodplain. *Journal of Hydrology*, *617*, 129073, https://doi.org/10.1016/j.jhydrol.2023. 129073.

Naghavi, M., Mohammadi, M. & Mahtabi, G. (2023b). The effect of building arrangement on the flow characteristics in meandering compound channels. *Journal of Environmental Management*, *331*(1), 117288, https://doi.org/10.1016/j.jenvman. 2023.117288.

Naghavi, M., Mohammadi, M. & Mahtabi, G. (2023c). Transverse Velocities and Vortices in Compound Meandering Channel: Effect of Building Arrangement in the Floodplains. *Journal of Hydraulic Structures*, *9*(3), 66-87.

Naghavi, M., Mohammadi, M. & Mahtabi, G. (2024). The effect of structures density in the banks of meandering rivers on the flow characteristics during floods. *Journal of Water and Irrigation Management*, 14(1), 123-139. (In Persian)

Pan, Y., Li, Zh., Yang, K. & Jia, D. (2019). Velocity distribution characteristics in meandering compound channels with one-sided vegetated floodplains. *Journal of Hydrology*, *578*, 1-11.

Pu, J.H. (2019). Turbulent rectangular compound open channel flow study using multi-zonal approach. *Environmental Fluid Mechanics*, *19*(3), 785-800.

Pu, J.H. (2022). Environmental Hydraulics, Turbulence and Sediment Transport. *Fluids, 7*(2), 48, https://doi.org/10.3390/fluids7020048.

Pu, J.H., Pandey, M., Li, J., Satyanaga, A., Kundu, S. & Hanmaiahgari, P.R. (2022). Editorial: Urban Fluvial and Hydro-Environment System. *Frontiers in Environmental Science*, *10*, 1-3.

Pu, J.H., Hussain, A., Guo, Y., Vardakastanis, N., Hanmaiahgari, P.R. & Lam, D. (2019). Submerged Flexible Vegetation Impact toward Open Channel Flow Velocity Distribution: An Analytical Modelling Study on Drag and Friction. *Water Science Engineering*, *12*(2), 121-128.

Pu, J.H., Shao, S. & Huang, Y. (2014). Numerical and experimental turbulence studies on shallow open channel flows. *Journal of Hydro-environmental Research*, *8*(1), 9-19.

Pu, J.H. (2015). Turbulence Modelling of Shallow Water Flows using Kolmogorov Approach. *Computational Fluids*, *115*, 66-74.

Sanjou, M. & Nezu, I. (2010). Large eddy simulation of compound open-channel flows with emergent vegetation near the floodplain edge. *Journal of Hydrodynamics*, *22*(5), 582-586.

Shiono, K. & Muto, Y. (1998) Complex flow mechanisms in compound meandering channels with overbank flow. *Journal of Fluid Mechanics*, *376*, 221–261.

Shiono, K., Chan, T.L., Spooner, J., Rameshwaran, P. & Chandler, J.H. (2009). The effect of floodplain roughness on flow structures, bedforms and sediment transport rates in meandering channels with overbank flows: Part I. *Journal of Hydraulic Research*, *47*, 5–19.

Shukla, D.R. & Shiono, K. (2008). CFD modelling of meandering channel during floods. *Proceedings of the Institution of Civil Engineers-Water Management*. *161*, 1–12.

Shukry, A. (1950). Flow around bends in an open flume. *Transactions of the American Society of Civil Engineers*, *115*(1), 751-779.

Tang, H., Tian, Z., Yan, J. & Yuan, S. (2014). Determining drag coefficients and their application in modelling of turbulent flow with submerged vegetation. *Advances in Water Resources*, *69*, 134-145.

Tsujimoto, T. (1992). Spectral analysis of velocity and water surface fluctuations appearing in an open channel with vegetated and non-vegetated regions in a cross-section. In: Proceedings of the sixth IAHR International Symposium on Stochastic Hydraulics, IAHR, Taipei.

Van, C.P., Deleersnijder, E., Bousmar, D. & Soares-Frazão, S. (2014). Simulation of flow in compound open-channel using a discontinuous Galerkin finite-element method with Smagorinsky turbulence closure. *Journal of Hydro-environmental Research*, *8*(40), 396-409.

Wang, M., Avital, E.J., Bai, X., Ji, C., Xu, D., Williams, J.J.R. & Munjiza, A. (2020). Fluid–structure interaction of flexible submerged vegetation stems and kinetic turbine blades. *Computational Particle Mechanics*, *7*, 839–848.

Wang, Y., Yang, Z., Liu, M. & Yu, M. (2022). Numerical study of flow characteristics in compound meandering channels with vegetated

floodplains. *Physics Fluids*, *34*(11), 115107, 10.1063/5.0122089.

Xu D, Bai Y, Munjiza A, Avital E, Williams J (2013) Investigation on the Characteristics of Turbulent Flow in a Meandering Open Channel Bend Using Large Eddy Simulation. In: Proceedings of 2013 IAHR World Congress, IAHR, China.

Yakhot, V., Thangam, S., Gatski, T.B., Orszag, S.A. & Speziale, C.G. (1992). Development of turbulence models for shear flows by a double expansion technique. *Physics Fluids*. *4*(7),1-24.

Zhang, H.T., Dai, W.H., da Silva, A.M.F., & Tang, H. (2022). Numerical study on resistance to flow in meandering channels. *Journal of Hydraulic Engineering*. *148*, 1–14.

Zhang, H.T., Dai, W.H., da Silva, A.M.F. & Tang, H.W. (2021). Numerical model for convective flow in meandering channels with various sinuosities. *Journal of Hydraulic Engineering*. *147*(11), 04021042, doi:10.1061/(asce)hy.1943-7900.0001917.